


## Article

# Micro-Scale Fracture Characteristics of Emulsified Asphalt Cold Recycled Mixture Based on Discrete Element Method

Yanhai Yang<sup>1</sup>, Yumeng Chen<sup>1</sup>, Baichuan Li<sup>2</sup>  and Ye Yang<sup>1,\*</sup>

<sup>1</sup> School of Transportation and Geomatics Engineering, Shenyang Jianzhu University, Shenyang 110168, China; yhyang@sjzu.edu.cn (Y.Y.); chenym1552@163.com (Y.C.)

<sup>2</sup> School of Transportation and Shipping, Wuhan University of Technology, Wuhan 430063, China; stephenlee183@163.com

\* Correspondence: yangye@sjzu.edu.cn

**Abstract:** Asphalt pavement often experiences structural failure due to repeated vehicle loading. The discrete element method (DEM) model was established based on the semicircle bending test (SCB) to investigate the fracture damage mechanism of emulsified asphalt cold recycled mixture (CRME) under loading. The micro-mechanical parameters of CRME were determined through a reliable validation process using the uniaxial compression static creep test. The microscopic fracture characteristics of CRME were investigated through the load-displacement curve, stress distribution, and force chain distribution. The fracture energy was used as the evaluation index to analyze the influence of prefabricated notch length and aggregate gradation on the fracture performance of CRME. The results indicate that the emulsified asphalt mortar-aggregate interface was the critical weak position of the mixture fracture; the failure of the tension chain was the main destructional form of the SCB test. The development of cracks affected the stress concentration phenomenon and stress concentration level of the mixture. Fine-grained mixture exhibited crack resistance. The number and length of cracks were affected by gradation. As the prefabricated notch length increased, the influence gradually diminished. The research results could provide theoretical and data support for the design of CRME.

**Keywords:** emulsified asphalt cold recycled mixture; discrete element; fracture characteristics; micro-scale



**Citation:** Yang, Y.; Chen, Y.; Li, B.; Yang, Y. Micro-Scale Fracture Characteristics of Emulsified Asphalt Cold Recycled Mixture Based on Discrete Element Method. *Coatings* **2024**, *14*, 1436. <https://doi.org/10.3390/coatings14111436>

Academic Editor: Paolo Castaldo

Received: 12 October 2024

Revised: 8 November 2024

Accepted: 9 November 2024

Published: 12 November 2024



**Copyright:** © 2024 by the authors. Licensee MDPI, Basel, Switzerland. This article is an open access article distributed under the terms and conditions of the Creative Commons Attribution (CC BY) license (<https://creativecommons.org/licenses/by/4.0/>).

## 1. Introduction

The cold recycled asphalt mixture (CRME) is formed by stabilizing recycled asphalt with emulsified asphalt as a binder. It includes appropriate amounts of mineral powder, cement, and other fillers, and may also incorporate a specific proportion of new aggregates or additives, mixed with water as needed. Because of low carbon and environmental-protection characteristics, CRME have been widely used in high-grade highway bases, ordinary highway surfaces, or bases internationally [1–3]. However, the combined effects of temperature, moisture, freezing, and thawing affects the mechanical properties of asphalt mixture [4,5]. Under the influence of load and temperature stresses, micro cracks within the CRME propagate along the interface transition zone. This process initially manifests as the initiation, development, and penetration of micro cracks, eventually leading to the formation of macrocracks, which results in cracking of the cold recycled pavement [6]. Through fracture test and numerical simulation, Yu et al. found that cracks always develop along the weak interface transition zone. It is the aggregate in the fracture trend zone that makes the fracture path tortuous, and the bending and shear stress around the aggregate will change substantially [7]. Loria et al. evaluated the performance of various emulsified asphalt cold recycled sections in Nevada. The use of CRME could effectively reduce the number of reflective cracks on the pavement [8]. Morian et al. found that the crack resistance of emulsified asphalt cold recycled pavement is two to three times that of traditional hot mix asphalt

mixture, and the material cost is only two-thirds of that of hot mix asphalt mixture [9]. Zhang et al. found that the regenerant significantly influenced the low-temperature crack resistance of CRME through the semicircle bending test (SCB) [10]. Wang et al. discovered that the bending tensile stress and fracture energy density of CRME were improved after adding regenerate and styrene-butadiene latex [11]. Barghabany et al. detected that the asphalt mixture with high RAP content leads to a decrease in the crack resistance of the mixture through the component analysis and semi-circular bending test of the asphalt mixture [12]. Ma obtained that reasonable RAP content is conducive to improving the crack resistance of CRME through laboratory tests [13]. Flores et al. found that cement contributes to enhance the water-damage resistance of CRME [14]. Zhang et al. predicted that the virgin mixtures and those with soft base binders will have better capability to resist cracking after long-term aging through fracture tests and pavement evaluation [15]. Feng et al. established the relationship between pavement cracking spacing and asphalt mixture fracture energy, fracture toughness, and modulus of elasticity through the SCB test [16]. As mentioned above, various methods have been employed in indoor experiments to analyze the crack-resistance performance of CRME. These methods could provide certain guidance for practical pavement engineering applications. However, relying solely on phenomenological analysis of the performance of CRME could not explain the fundamental causes of mixture fracture from the microscopic and mechanical perspective. Therefore, experts and scholars internationally tried to explore the micro-mechanical properties of the mixture under different conditions from the micro-perspective.

The discrete element method (DEM) based on particle flow overcomes the defect that the finite element method could not reflect the interaction among particles. The pavement materials are composed of particle flow with strong discreteness, widely used in the road field [17–19]. The components of the mixture could be clearly distinguished in the DEM. The distribution of the micro-scale contact force chain in the specimen and the corresponding macroscopic performance index could be accurately detected. The change of displacement with load could serve as the basis for judging the structural performance of the material [20–22]. Wu et al. established a two-dimensional skeleton model through DEM and explored the influence of gradation segregation on the internal skeleton structure and stress characteristics of the asphalt mixture [23]. Liu et al. used DEM to establish the pavement compaction model and analyzed the micro-mechanical behavior in pavement compaction. The author concluded the discrete element model was reasonable and feasible [24]. Shi et al. conducted the stress ratio transmitted by the skeleton is proportional to the nominal maximum particle size of the aggregate and inversely proportional to the thickness of the specimen through DEM research [25]. Zhang et al. carried out the three-dimensional Discrete Element Method virtual uniaxial creep test of asphalt mixture. The accuracy of the three-dimensional creep test was verified by comparing with the indoor test [26]. Yu et al. simulated the complex modulus of asphalt mixture by developing three-dimensional DEM, and successfully predicted the dynamic modulus and phase angle of the dense-graded asphalt mixture at different temperatures and frequencies [27]. Huang et al. obtained that DEM was the new method to study the temperature field distribution of the mixture by reconstructing the digital sample of the rutting plate [28]. The early DEM model offered initial insights into the fundamental influences of aggregate gradation, shape, and contact mechanics on the performance of asphalt mixtures. However, these models do not allow the examination of complex aggregate microstructures or aggregate crushing modeling during strength test simulations. The FEM of asphalt concrete microstructure could simulate the geometry of aggregate and asphalt mortar microstructure accurately. However, the current limitation of this method could not simulate the changing aggregate contact geometry (aggregate contact and detachment or sliding during loading). In addition, modeling the fracture of aggregates or blocks during strength test simulations is particularly challenging. William G et al. described a discrete element method (MDEM), which balances the advantages of the resolution of the microstructure model with the ability to deal with changing contact conditions and fractures. This technique was the

direct extension of the traditional DEM analysis, in which various material phases (such as aggregates, adhesives) were modeled with very small discrete element groups. The MDEM method possessed all the advantages of traditional DEM, such as the ability to handle complex and constantly changing contact geometries, as well as the applicability of simulating large displacement and crack propagation. The method could simulate aggregates with small discrete elements forming a “mesh” and model complex aggregate shapes as well as crack propagation around or through aggregates during strength testing [29]. Barghabany et al. utilized artificial neural network to establish the SCB prediction model of asphalt mixture fracture parameters. The results indicated that compared to traditional linear and nonlinear regression models, the artificial neural network method has been proven effective in predicting the fracture energy of the asphalt mixture [30].

On the basis of the existing results, based on the SCB test, the micro-fracture characteristics of CRME are explored by DEM. The main parts include the following: The aggregate template was obtained by real cross-section vectorization. The discrete element model of CRME was constructed. The micro-mechanical calculation parameters were determined through a combination of empirical trial-and-error methods and indoor test. The fracture process of the SCB test mixture was explored from the perspective of load-displacement curve, stress distribution, and force chain distribution. The influence of aggregate gradation and prefabricated notch on the fracture performance of the mixture was investigated, and the fracture energy was used as the evaluation index. The effect of the prefabricated notch on the number and length of cracks in the SCB test was investigated.

## 2. Laboratory Test and Discrete Element Model

### 2.1. Raw Materials

The RAP was derived from the surface layer of the highway. The asphalt was slow-cracking cationic emulsified asphalt. According to the relevant requirements in the ‘Technical Specification for Regeneration of Highway Asphalt Pavement’ (JTG/T 5521-2019) [31], combined with the use conditions and actual engineering feedback, some limestone alkaline new aggregates were added to meet the grading requirements of medium-grained CRME. The results of the RAP performance test are shown in Table 1 and the emulsified asphalt performance test results are shown in Table 2. The designed aggregate gradation curve is illustrated in Figure 1. All materials meet the requirements of the current Chinese specifications ‘Technical Specification for Construction of Highway Asphalt Pavements’ (JTG F40-2004) [32] and ‘Technical Specification for Regeneration of Highway Asphalt Pavement’ (JTG/T 5521-2019).

**Table 1.** RAP performance test results.

Index	Test Result	Technical Requirement
Moisture content/%	0.85	≤3
Asphalt content/%	4.5	-
Sand equivalent/%	61.2	≥50

**Table 2.** Emulsified asphalt performance test results.

Index	Test Result	Technical Requirement
Residue content/%	64.0	≥60
Penetration (25 °C, 100 g)/0.1 mm	68.1	50~130
Ductility (15 °C)/cm	76.5	≥40
Solubility/%	99.1	≥97.5
Storage stability (5 d, 25 °C)/%	2.7	≤5

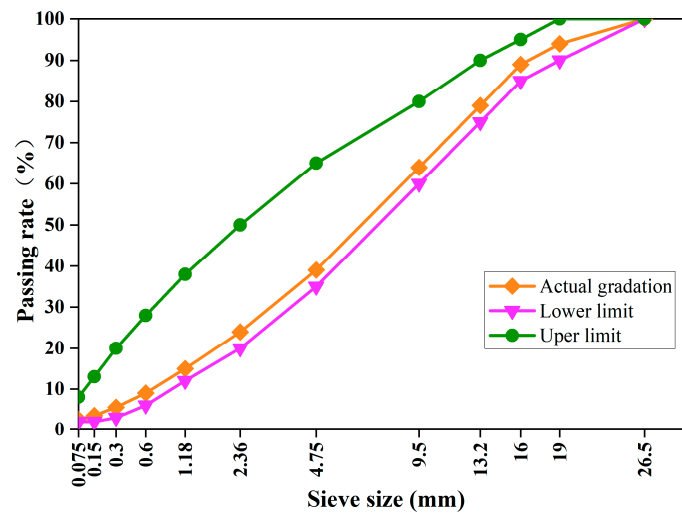


Figure 1. Design Aggregate gradation curve.

## 2.2. SCB Test

According to the 'Highway Engineering Asphalt and Asphalt Mixture Test Procedures' (JTG E20-2011) requirements [33], the emulsified asphalt cold recycled specimen was formed by AFG2 C rotary compactor. The compaction height is 63.5 mm, or the compaction times are 100 times. After forming, the mixture specimens are placed in the 60 °C blast oven for 48 h to constant weight. The specimens, after curing, were placed at room temperature for 12 h and then cut into semi-circular disc specimens after strength formation. The SCB indoor loading test is shown in Figure 2. The bottom support distance is 0.8 times the diameter of the specimen, and the loading rate is 50 mm·min<sup>-1</sup>. The temperature is controlled at about −10 °C.



Figure 2. Semi-circular bending laboratory test.

## 2.3. Numerical Model Construction

### 2.3.1. Construction of the Aggregate Model

The coarse aggregate of asphalt mixture was usually irregular [34]. To keep the numerical simulation of aggregate characteristics consistent with the actual situation, a two-dimensional aggregate template was obtained by combining indoor specimens with numerical simulation. The method was as follows: The sample was cut to obtain a sample suitable for subsequent test or analysis. Image preprocessing of the sample surface: including noise removal, contrast adjustment, grayscale normalization, edge enhancement, and other methods. The image was first binarized by Matlab2016a, the image was converted into an image with only two colors (usually black and white) and then vectorized to obtain the shape, size, boundary characteristics, and other information of the aggregate, and the aggregate contour template was obtained. The discrete element software was introduced to

simulate the accumulation and aggregation of particles through the Bubblepack algorithm. By simulating the collision and interaction of particles, the particles were automatically aggregated into clusters (Clump) according to certain rules. The generated Clump structure could more realistically simulate the aggregate distribution and interaction in the actual mixture and provide a reliable basis for subsequent physical simulation and mechanical performance analysis [35]. The steps are shown in Figure 3.

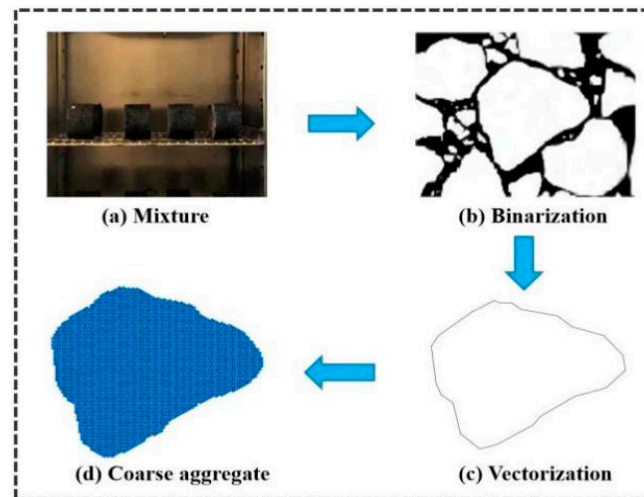


**Figure 3.** Establishment process of the coarse aggregate model.

### 2.3.2. Specimen Model Construction

The DEM has shown significant advantages in the crack analysis of the asphalt mixture. The core of DEM is that it could accurately simulate the behavior and interaction of particles in the material. This detailed particle modeling enables researchers to deeply understand the propagation mechanism of cracks, especially when dealing with discontinuous and local failure of materials. DEM could effectively simulate the formation and propagation of cracks. In addition, researchers could flexibly adjust the model parameters according to the actual material properties, so that the simulation results are closer to the real situation and the prediction accuracy is improved. CRME mainly comprises RAP, new aggregate, and emulsified asphalt mortar [36]. To improve the computational efficiency of the Discrete Element Method model and the acquisition of micro-scale parameters, 2.36 mm was used as the boundary to distinguish the different components. Aggregate with a particle size greater than 2.36 mm is regarded as coarse aggregate and selected from the aggregate template. Aggregates with particle size of less than 2.36 mm are regarded as continuous medium asphalt mortar. The asphalt mortar was generated by replacing the ball with a radius of 0.1 mm, and the voids between the spheres were regarded as voids. Due to the minor impact of loading rate on fracture characteristics [37], the numerical simulation of the upper indenter loading rate and the bottom bearing spacing were consistent with the laboratory test. Therefore, the mixture discrete element model with gradation characteristics was constructed, as shown in Figure 4. To ensure that the gradation of the numerical model was consistent with the actual, the model was constructed according to the volume percentage PV of each mineral aggregate. The PV of emulsified asphalt mortar was 31.8%, and the volume percentage of each coarse aggregate is shown in Table 3.

**Table 3.** Coarse aggregate volume percentage.

Sieve Size/mm	26.5~19.0	19.0~16.0	16.0~13.2	13.2~9.5	9.5~4.75	4.75~2.36
New aggregate PV/%	1.8	1.5	3	4.5	7.5	4.5
RAP PV/%	-	1.68	1.89	5.73	21	15.1



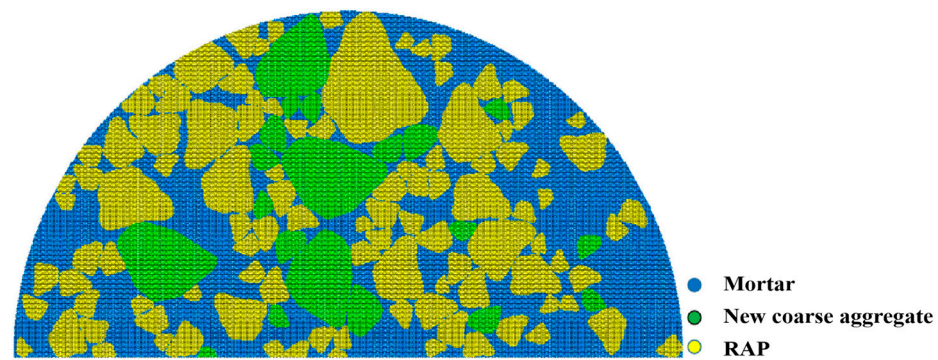


**Figure 4.** Two-dimensional mixture numerical specimen.

## 2.4. Contact Constitutive Model and Parameter Determination

### 2.4.1. Introduction of Contact Constitutive Model

In the discrete element software (PFC5.0), the response mode between the contact discrete units was determined by the connection mode. The motion state of the whole specimen was obtained through iterative calculation based on the interaction between the discrete units. The built-in contact modes of the software were divided into two types. One type describes only the compressive state of the contact, while the other type describes the adhesive state. The embedded contact models of the program included linear contact bond model, parallel bond model, and Burger's model.

The linear model could be used to describe the relationship between the standard and tangential contact forces and relative displacements between discrete bodies, and mechanical behavior was based on the linear elastic law and viscous damping. The linear contacted bond model regarded the contact bond as a bond point. The contact was destroyed if the normal force exceeded the normal bond strength. If the shear force exceeded the shear strength, the contact was destroyed, but the contact force was not changed. The contact model was destroyed and regressed into a linear model. The parallel bond model described the mechanical behavior of the bonding material. The bonding component was parallel to the linear element, and the elastic interaction was established between the contacts. The contact model was degenerated into a linear model after failure. The Burger's model comprised the Kelvin and Maxwell models in series in the normal and tangential directions to simulate the creep mechanism between particles.

### 2.4.2. Micromechanical Parameters

Coarse aggregates, as relatively hard materials, are considered as internally unbreakable rigid bodies in the discrete element model, represented by Clumps, without the need for internal contacts. Therefore, there were mainly three kinds of contacts in the micro part of CRME. As shown in Figure 5, these contacts include the contact between emulsified asphalt mortar units, the contact between aggregate units, and the contact between aggregate and emulsified asphalt mortar.

Therefore, in the discrete element model, the contact between the emulsified asphalt mortar units adopted the Burger's model and the parallel bond model. The contact between the aggregate units adopted the linear contact bond model, and the aggregate and the emulsified asphalt mortar adopted the Burger's model and the parallel bond model. Figure 6 depicts the schematic diagram of the linear contact bond model and the parallel bond model in the activated state. Figure 7 illustrates the Burger's model describing the asphalt mortar's macroscopic and microscopic properties.

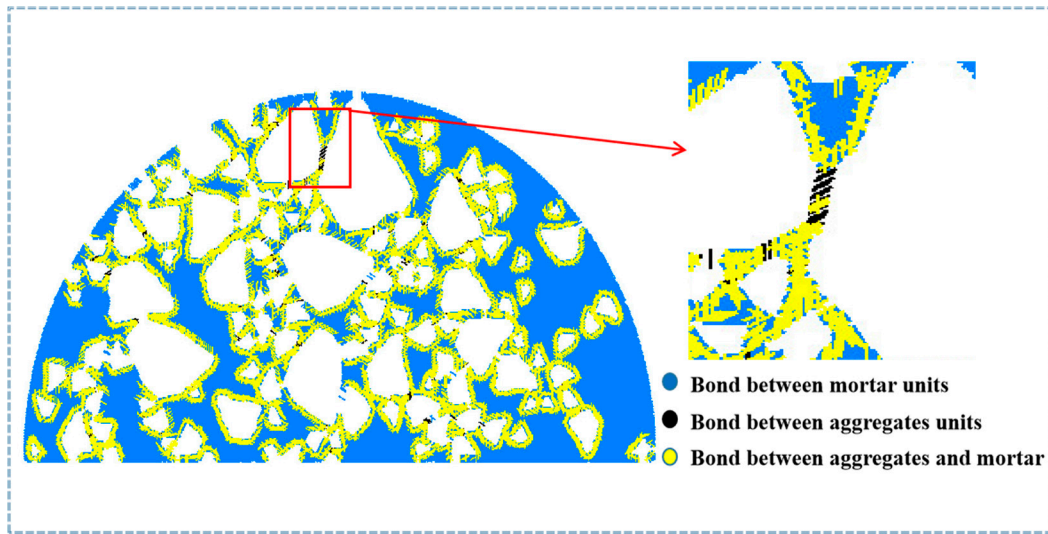


Figure 5. Contact type of numerical specimen.

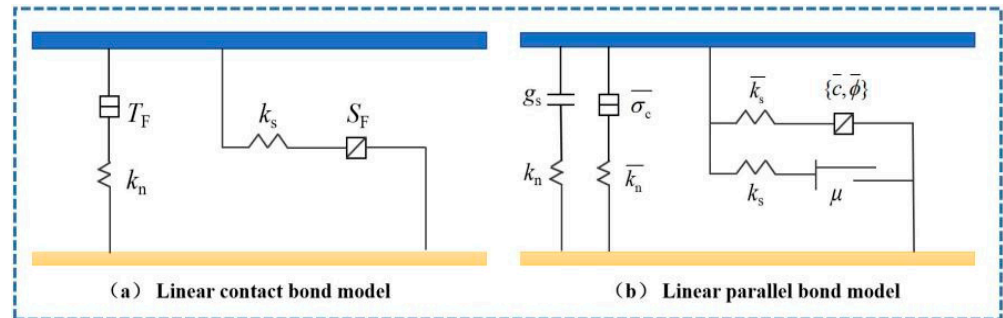


Figure 6. The schematic diagram of the bond mechanical model of CRME.

Static creep tests were conducted on emulsified asphalt mortar at 15 °C, and the experimental data was subjected to nonlinear fitting (as shown in Figure 8). The micro-scale Burger’s model parameters of emulsified asphalt mortar could be determined by the fitting results (As shown in Table 4). According to Equations (1)–(3), and referenced to the corresponding research results [38–40], the micro-scale parameters required for calculation were obtained, as shown in Tables 5 and 6.

Table 4. Macroscopic Burger’s model parameters of emulsified asphalt mortar.

$E_1/\text{MPa}$	$E_2/\text{MPa}$	$\eta_1/\text{MPa}\cdot\text{s}$	$\eta_2/\text{MPa}\cdot\text{s}$
274.51	79.84	72074.9	2498.32

$$J(t) = \frac{\varepsilon(t)}{\sigma_0} = \frac{1}{E_1} + \frac{t}{\eta_1} + \frac{1}{E_2} \left(1 - e^{-\frac{E_2 t}{\eta_2}}\right) \tag{1}$$

$$K_{mn} = 2E_1L, K_{ms} = \frac{E_1L}{(1+V)}, K_{kn} = 2E_2L, K_{ks} = \frac{E_2L}{(1+V)} \tag{2}$$

$$C_{mn} = 2\eta_1L, C_{ms} = \frac{\eta_1L}{(1+V)}, C_{kn} = 2\eta_2L, C_{ks} = \frac{\eta_2L}{(1+V)} \tag{3}$$

where:  $J(t)$  is the creep compliance at any time,  $\varepsilon(t)$  is the strain at any time,  $\sigma_0$  is the static constant load stress level,  $E_1, E_2, \eta_1, \eta_2$  are the macro-scale mechanical parameters of Burger’s model,  $K_{mn}, K_{ms}, K_{kn}, K_{ks}, C_{mn}, C_{ms}, C_{kn}$  and  $C_{ks}$  are the micro-scale mechanical parameters of Burger’s model,  $L$  is the center distance of adjacent elements, and  $V$  is the normal tangential stiffness ratio of asphalt mortar [41–43].

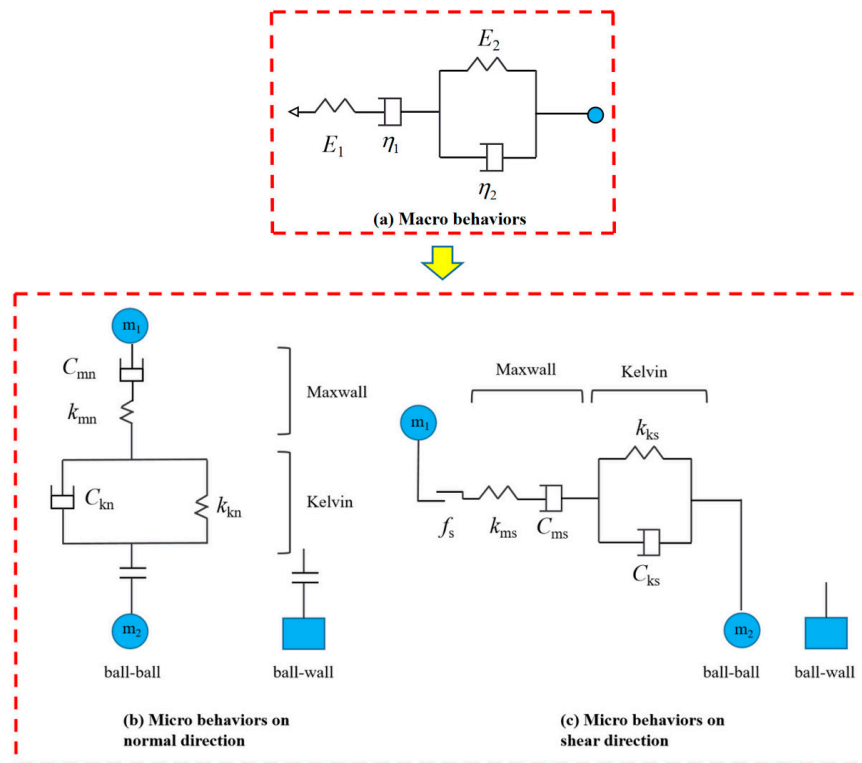


Figure 7. The schematic diagram of the Burger's mechanical model of asphalt mortar.

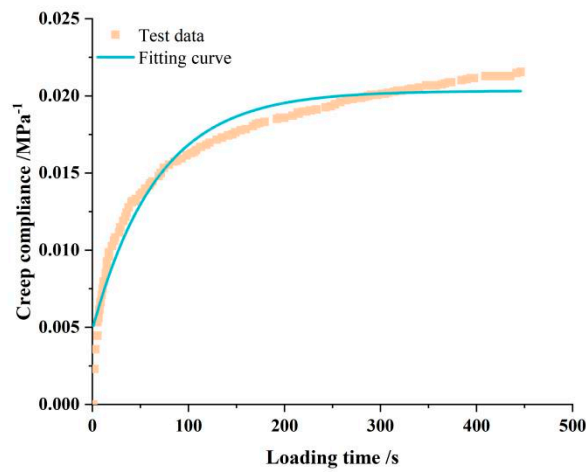


Figure 8. Creep compliance test and fitting curve.

Table 5. Parameters of mixture micro-scale Burger's model.

	$K_{mn}/\text{Pa}$	$K_{kn}/\text{Pa}$	$C_{mn}/\text{Pa}\cdot\text{s}$	$C_{kn}/\text{Pa}\cdot\text{s}$	$K_{ms}/\text{Pa}$	$K_{ks}/\text{Pa}$	$C_{ms}/\text{Pa}\cdot\text{s}$	$C_{ks}/\text{Pa}\cdot\text{s}$
Mortar	$4.98 \times 10^6$	$1.44 \times 10^7$	$1.59 \times 10^5$	$5.49 \times 10^5$	$2.00 \times 10^6$	$5.77 \times 10^7$	$6.39 \times 10^5$	$2.19 \times 10^5$
Aggregate-mortar	$3.74 \times 10^6$	$1.08 \times 10^7$	$1.11 \times 10^5$	$4.11 \times 10^5$	$1.49 \times 10^6$	$4.32 \times 10^7$	$4.79 \times 10^5$	$1.64 \times 10^5$

Table 6. Parameters of meso-parallel bond model of mixture.

	Effective Modulus $e_{mod}/\text{Pa}$	Tensile Strength $\sigma_c/\text{Pa}$	Shear Strength $c/\text{Pa}$	Friction Coefficient $f$	Normal to Shear Stiffness Ratio
Mortar	$2.13 \times 10^6$	$2.36 \times 10^5$	$3.50 \times 10^5$	0.25	1
Aggregate-mortar	$2.00 \times 10^6$	$2.18 \times 10^5$	$3.10 \times 10^5$	0.25	2.4



In view of the complexity of RAP materials, there are many challenges in accurately determining the contact parameters between RAP and asphalt mortar. However, RAP is similar to the new aggregate in nature, and there may be slight differences in physical properties. In order to improve the computational efficiency and maintain the operability of the model, the RAP-emulsified asphalt mortar contact and the new aggregate-emulsified asphalt mortar contact are simplified to the same contact. The interface weakening coefficient was 75% between emulsified asphalt mortar and aggregate [37]. After determining the test correlation coefficients, the model was used for micro-scale experimental validation. The experimental results were compared with macro-scale test data to verify the accuracy and reliability of the model. The comparison between the simulation test results and macro-scale test data is shown in Figure 9. It could be seen from Figure 9 that compared with the macro-scale indoor test, the error of the micro-scale test was relatively small. The splitting strength was close, the load displacement curve was consistent after the peak, and the micro-scale parameters of the model had certain reliability.

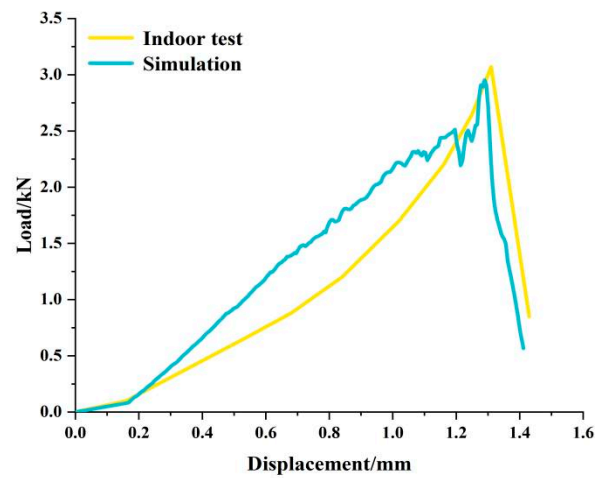


Figure 9. SCB test load-displacement diagram.

### 3. Results and Discussion

#### 3.1. Analysis of 2D-SCB Virtual Fracture Process

The early fracture failure process of the SCB test is shown in Figure 10. It could be seen from Figure 10 that the crack tip of the specimen with a prefabricated notch length of 10 mm (Area 1 in Figure 10b) first initiated cracks and gradually extended upwards. Due to the blocking effect of large particle aggregate at the center of the specimen, the cracks further gathered in the area 2 of Figure 10b. The aggregate-mortar interface in the area 3 of Figure 10b gradually reached its tensile strength and fractures. As the loading progressed, the crack extended to the upper part of the specimen and formed a main crack.

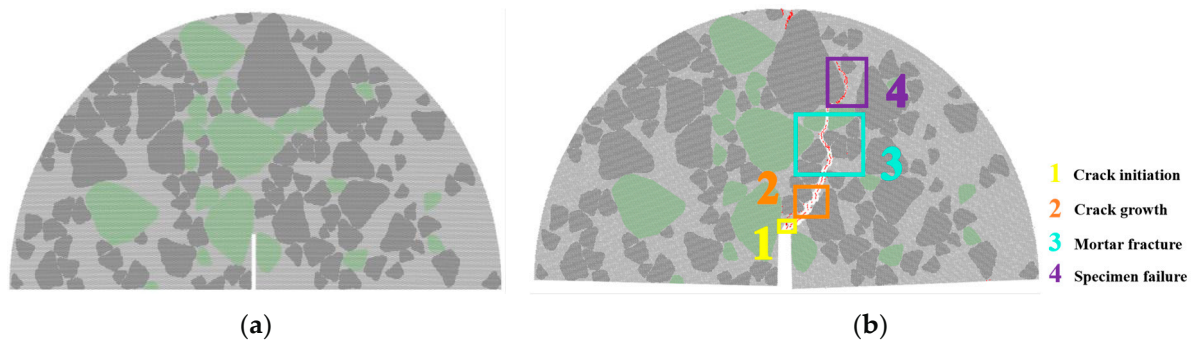
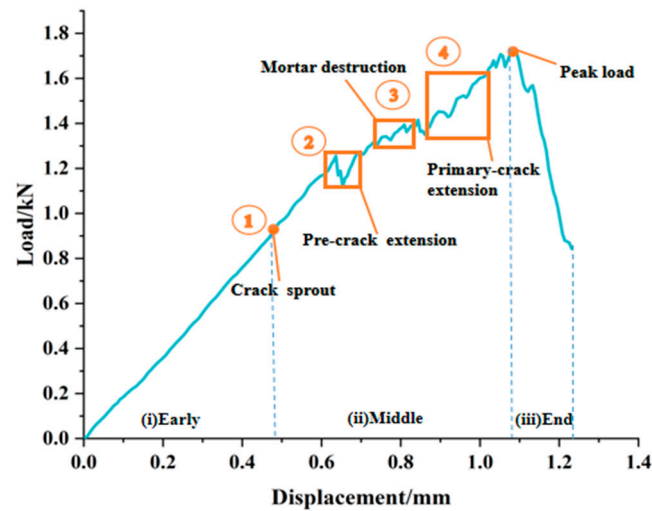


Figure 10. Fracture path of SCB test: (a) Before damage; (b) After damage.

The corresponding relationship between the actual fracture position of the SCB specimen and the load-displacement curve during the loading process is shown in Figure 11. It could be seen from Figure 11 and Formula (4) that the bending stiffness index of the SCB specimen was 1.883 kN/mm and the bending strength was 164.16 MPa. The pre-peak fracture energy was 25.5 N/mm, and the post-peak fracture energy was 4.25 N/mm. The peak load was 1.71 kN, and the corresponding fracture displacement was 1.05 mm.

$$G_f = W_f / A_{lig} \quad (4)$$

In the formula:  $W_f$  is the work of fracture,  $W_f = \int P du$ ,  $P$  is the applied load,  $u$  is the average load line displacement,  $A_{lig}$  is the ligament area,  $A_{lig} = (r-a)t$ ,  $r$  is the radius of the sample,  $a$  is the length of the incision, and  $t$  is the thickness of the sample.



**Figure 11.** Test load displacement curve and fracture position corresponding diagram.

From the comparative analysis of the load-displacement curve and the fracture position, it could be determined that the fracture performance of the material was affected by the work done by the external force, and the fluctuation of the load-displacement curve was closely related to the interface fracture. The load curve fluctuates slightly when the crack initiates. The second fluctuation was that the crack in the area 2 in Figure 10b further expands, and the fluctuation range was extensive. In the third fluctuation, due to the blocking effect of large particles, both sides of the coarse aggregate became the possible path of crack development. The cracks gradually extended along the mortar-aggregate interface. The emulsified asphalt mortar was broken and damaged, corresponding to the area 3 in Figure 10b. Before the peak load, the load curved fluctuates for the fourth time, and the primary cracked forms and expanded until the specimen was destroyed. This indicated that before the cracks of the CRME occur, the work done by the external force was distributed in each part of the specimen, causing them to produce different degrees of deformation.

Once the crack occurs, the work done by external force mainly concentrated in the crack part, causing the crack to expand sharply. This was consistent with the microscopic damage results of a cold recycled mixture under freeze-thaw cycles based on the discrete element model by Li et al. [44]. This phenomenon was also reflected in the stress-distribution cloud diagram of the specimen. The stress cloud diagram of the loading process of the specimen is shown in Figure 12. It could be seen from Figure 12 that the development of the crack path was always dynamic, and the cracks' generation makes the mixture's internal stress change significantly. After the mixture cracks, stress concentration occurred near the cracks, weakening the bonding effect between the aggregate and the mortar in the surrounding area, and cracks were more likely to occur. The specimen's stress concentration was not

apparent when the crack was not generated at the initial loading stage. In the middle of the experiment, cracks appeared in the middle of the specimen, resulting in apparent stress concentration in the middle of the specimen. At the end of the test, the crack propagated to form the main crack, and the fracture part of the specimen showed an apparent unloading phenomenon, but there was still a specific stress concentration in the unbroken part. This was consistent with the experimental results obtained by Wang et al. through the SCB test [45].

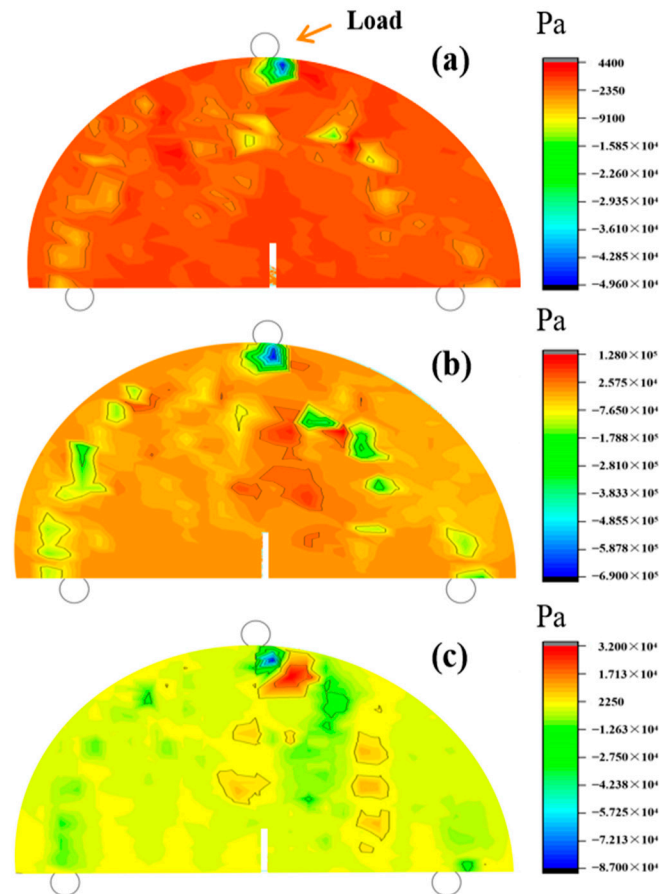


**Figure 12.** The stress-distribution diagram of the specimen: (a) Early stage of the test; (b) Middle stage of the test; (c) End stage of the test.

The internal force chain distribution of the specimen also changed due to the fracture of the specimen. Figure 13 illustrates the distribution of the internal force chain of the three-stage loading specimen. It could be seen from Figure 13a that the tension chain of the specimen was mainly distributed between the two supports, the pressure chain was mainly distributed at the fulcrum and load, and an arched pressure band was formed at the periphery of the semi-circular specimen along the fulcrum. In the middle of the test (Figure 13b), the tensile chain of the weak interface at the aggregate-mortar interface was gradually destroyed by the external force, and the tensile chain between the mortar units gradually lost its function. The crack or pressure chain gradually replaced it. At the end of the experiment (Figure 13c), the failure of the specimen was divided into two parts, and the tension chain was dispersed in the center of the failure specimen. The main crack was formed between the prefabricated crack in the center of the specimen and the upper indenter. The main tensile chain in the center of the specimen was damaged, and the pressure chain became the main form of action inside the specimen.

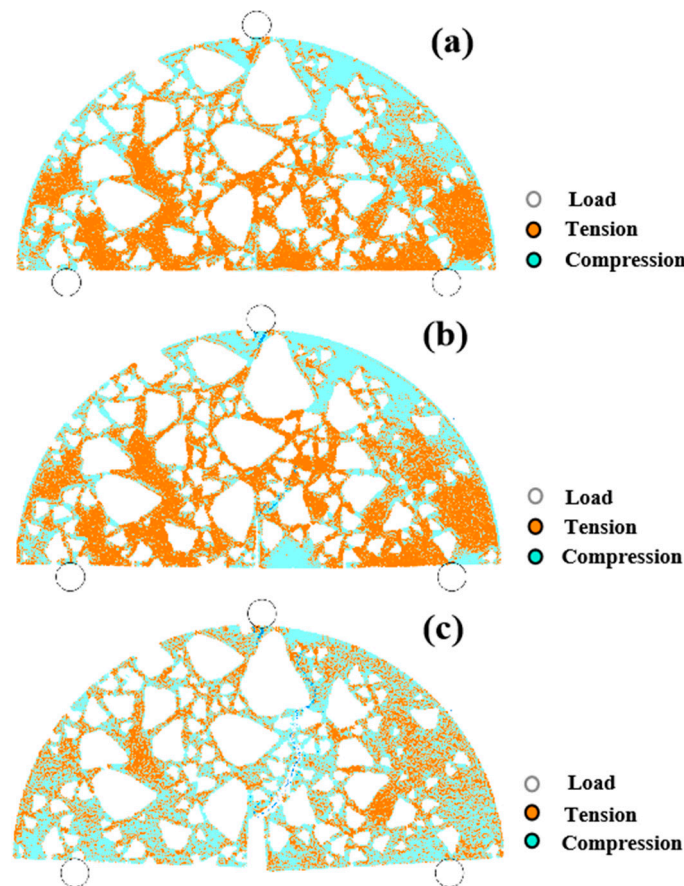


**Figure 13.** The internal force chain distribution of the specimen: (a) Early stage of the test; (b) Middle stage of the test; (c) End stage of the test.

### 3.2. Influence of Aggregate Gradation

Fracture mechanics believed that the material was destroyed when the external force was equal to the fracture energy of the material. The initiation of cracks and the generation of main cracks were the main forms of damage after the mixture was subjected to external loads. At the micro-scale, cracks occur as a result of the failure of the mechanical bond model between two discrete elements, leading to the generation of fracture cracks at the site of failure. In the splitting test, the selection process of CRME crack path was dynamic in nature. In areas of high stress and strain concentration, cracks tend to propagate in the direction that requires the least energy for them to propagate and eventually form the main fracture path. As the main component of the mixture resisted the external force, the aggregate played a decisive role in the fracture characteristics of the mixture. In order to investigate the influence of aggregate gradation and prefabricated notch length on the fracture energy of specimens, the experimental gradation was divided into coarse-grained type A, medium-grained type B, fine-grained type C, and original gradation D. The specific gradation composition is shown in Table 7. The relationship between fracture energy and prefabricated notch length is illustrated in Figure 14.

It could be seen from Figure 14 that the larger the length of the prefabricated notch, the smaller the fracture energy of the mixture and the weaker the crack resistance. Intuitively, as the notch depth increased, the fracture energy of the specimen gradually decreased, and this change tended to be linear [46,47]. This was because with the increase of the notch depth, the greater the material loss of the specimen, the lower the ability of the specimen to resist the external load, and the less work required for the specimen to be destroyed by the external load. Comparing the fracture energy of the mixture under different gradations, it could be concluded that the gradation significantly influenced the crack resistance of the mixture. The fracture performance of fine-grained mixture was superior compared to other

gradation types, with coarse-grained mixtures exhibiting poorer fracture performance. This was mainly attributed to the dense and uniform distribution of hard aggregates in the fracture surface of fine-grained mixtures, leading to stronger interactions among aggregates. The interaction among aggregates was the primary way to resist external forces. Furthermore, due to the less distribution of fine-grained mixture mortar, there were fewer branching fracture paths at the interface, leading to an overall increase in interface strength. Although the coarse-grained mixture was distributed with larger aggregates, the weak mortar interface also increased. The weak interface generated by the specimen under the action of external force was mainly distributed in the mortar interface, and the overall fracture performance was inferior.

**Table 7.** Three different types of aggregate gradation.

Sieve Size/mm	Sieve Pass Rate/%		
	Coarse A	Medium-Grained B	Fine-Grained C
37.5	100	—	—
26.5	90	100	—
19	85	95	100
16	76.5	90	95
13.2	70	82.5	90
9.5	55	70	70
4.75	42.5	50	60
2.36	30	35	40
1.18	21.5	25	27.5
0.6	15.5	17	19.5
0.3	11.5	11.5	15.5
0.15	6.5	7.5	9.5
0.075	4	5	5.5

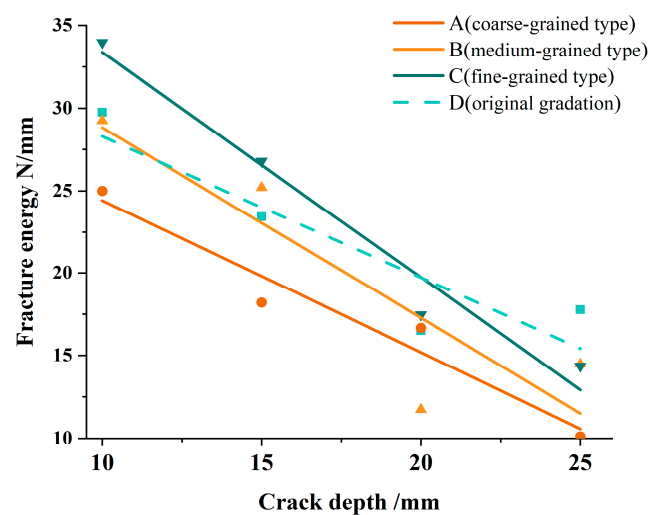


**Figure 14.** Relationship between fracture energy and prefabricated notch length.

### 3.3. Fracture Cracked

According to the failure characteristics of discrete element software contact model, the contact model failure was mainly divided into tensile failure and shear failure. In this exploration, the Fish command was used to monitor the model's failure mode and crack length at peak load for comparison among 16 sets of experimental crack types. The results are shown in Table 8. It could be seen from Table 8 that the failure mode between discrete elements was mainly tensile failure. From the type of crack and the proportion of crack length, the influence of shear crack could be ignored. This article focuses on the influence of tensile cracks on mixtures' cracking behavior.



**Table 8.** Mixture crack type distribution.

	Total Number of Cracks	Total Crack Length/mm
Tensile crack	1099	227.4
Shear fissure	5	1.4
Grand total	1104	228.8

The changes in the number and length of tensile cracks during the fracture process are shown in Figure 15. The comparison between Figure 15a and Figure 15b in Figure 15 reveals that the variation trend of crack number is basically consistent with that of crack length. Both the number and length of cracks gradually decreased as the pre-cut depth increased. Due to the hindrance of large coarse aggregate to the crack path, the crack had to bypass the sizeable coarse aggregate to find the optimal failure path, significantly increasing the number of failure cracks in coarse-grained and medium-grained mixtures. These observations were consistent with the conclusions obtained by Zhao et al. through the micro-cracking simulation of the mixture [48]. However, when the prefabricated notch was 20 mm or 25 mm, the force chain at the center of the specimen was reduced, and the overall tensile strength of the specimen was weak. The above phenomenon was not apparent, and the three graded mixtures exhibited very similar crack-development patterns. This implies that when the prefabricated notch was small, the overall tensile strength of the specimen was higher, the aggregate gradation affects the path of crack generation, and the specimen had a crack-development process of initiation-expansion-formation of primary crack-slow failure. When the prefabricated notch was large, the sensitivity of the crack to the gradation was reduced. The increased notch depth reduced the space for the formation of the main crack. The increment of the fracture surface formed by the prefabricated notch was much larger than that of the fracture surface in the experiment. The development process of the crack had the characteristics of rapid initiation-propagation-failure.

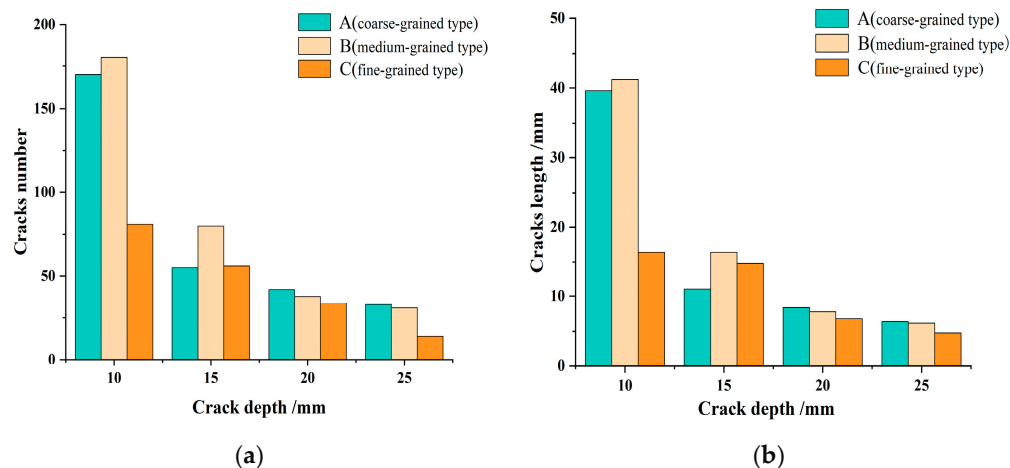


**Figure 15.** Changes in the number and length of tensile cracks during the fracture process of each type of asphalt mixture: (a) Quantity change; (b) Length change.

#### 4. Conclusions

Based on the indoor test, the discrete element model was used to carry out the numerical simulation analysis of the fracture characteristics of the CRME, and the fracture performance of the CRME was studied. The main conclusions were as follows:

(1) Based on the basic principle of DEM and the characteristics of the built-in contact model of discrete element software, it was feasible to use the macro-micro parameter conversion and the macro-micro comparison experiment to determine the micro-parameters of the discrete element, and the established CRME model had particular effectiveness.

(2) In the SCB test, the fluctuation of the load-displacement curve was affected by the interface cracking behavior. The stress-concentration phenomenon was related to the

development path of the crack. The failure of the tension chain was the primary failure mode in the fracture process of the mixture. When the external force exceeded the bearing range of the specimen and the main tension chain in the center of the specimen was damaged, the pressure chain became the main form of action inside the specimen.

(3) This model could be used to predict and evaluate the fracture performance of the mixture under different gradations. After comparison, it was concluded that the fracture energy decreases with the increase of the prefabricated notch length of the mixture, which tended to change linearly. The mixture's gradation composition significantly affected the fracture performance of the CRME. The fine-grained mixture had better fracture performance due to the dense and uniform distribution of aggregate and less weak mortar interface. The research method is reasonable, and the conclusion is reliable. The data obtained could provide theoretical guidance and data support for the study of different graded mixtures.

(4) The main crack form of the SCB test was a tensile crack, and the quantity and length of tensile cracks were affected by the type of aggregate gradation. When the prefabricated notch length was 10 mm, the crack length of coarse-grained and medium-grained mixtures was more significant. With the increase of the prefabricated notch length of the mixture, the sensitivity of the crack to the gradation decreased, and the quantity and length of the cracks produced by different gradations tended to be consistent.

(5) Because the coarse aggregate has a certain hindrance to the crack-propagation path, the strength of the emulsified asphalt mortar-aggregate interface was low and there was often a large stress concentration, which became the key weak link of crack propagation in the mixture. The crack resistance of CRME could be effectively improved by adding modified materials and improving aggregate surface treatment to enhance the cohesive strength of emulsified asphalt mortar and its bond strength with aggregate.

(6) In the discrete element model analysis based on the indoor test, the setting of parameters such as effective modulus, tensile strength, shear strength, and friction coefficient will affect the interaction between particles, and ultimately affect the fracture performance of the mixture. However, in order to comprehensively and deeply explore the fracture performance of CRME, a multi-index and multi-scale method could be used to improve the accuracy and prediction ability of the model by more accurately defining the contact parameters between RAP and asphalt mortar.

**Author Contributions:** Conceptualization, Y.Y. (Yanhai Yang) and Y.C.; Methodology, Y.C. and B.L.; Original draft preparation, Y.C.; Data curation, Y.C. and B.L.; Formal analysis, Y.Y. (Ye Yang); Writing—review and editing, Y.Y. (Yanhai Yang) and Y.Y. (Ye Yang); Supervision, Y.Y. (Yanhai Yang). All authors have read and agreed to the published version of the manuscript.

**Funding:** This research was funded by the National Natural Science Foundation of China (Grant No.52278454) and Shenyang Science and Technology Plan Project (Grant No.22322322).

**Institutional Review Board Statement:** Not applicable.

**Informed Consent Statement:** Not applicable.

**Data Availability Statement:** Data is contained within the article.

**Acknowledgments:** This research was performed at Shenyang Jianzhu University and Wuhan University of Technology.

**Conflicts of Interest:** The authors declare no conflict of interest.

## References

1. Yang, Y.H.; Wang, H.B.; Yang, Y.; Zhang, H.Z. Evaluation of the evolution of the structure of cold recycled mixture subjected to wheel tracking using digital image processing. *Constr. Build. Mater.* **2021**, *304*, 124680. [[CrossRef](#)]
2. Lin, J.T.; Huo, L.; Xu, F.; Xiao, Y.; Hong, J.X. Development of microstructure and early-stage strength for 100% cold recycled asphalt mixture treated with emulsion and cement. *Constr. Build. Mater.* **2018**, *189*, 924–933. [[CrossRef](#)]
3. Yang, Y.; Sun, Z.G.; Yang, Y.H.; Yue, L.; Chen, G.L. Effects of freeze–Thaw cycles on performance and microstructure of cold recycled mixtures with asphalt emulsion. *Coatings* **2022**, *12*, 802. [[CrossRef](#)]

4. Bazuhair, R.W.; Howard, I.L.; Middleton, A.; Jordan III, W.S.; Cox, B.C. Combined Effects of Oxidation, Moisture, and Freeze–Thaw on Asphalt Mixtures. *Transp. Res. Rec.* **2020**, *2674*, 409–424. [[CrossRef](#)]
5. Wang, Y.; Yang, X.; Jiang, J.B.; Li, P.; Nian, T.F. Mesoscopic process of water damage development of asphalt mixture in seasonal frozen area under scouring action of dynamic water. *Mater. Bull.* **2022**, *36*, 50–56.
6. Ding, X.H.; Ma, T.; Gu, L.H.; Zhang, Y. Investigation of surface micro-crack growth behavior of asphalt mortar based on the designed innovative mesoscopic test. *Mater. Des.* **2020**, *185*, 108238. [[CrossRef](#)]
7. Yu, J.J.; Li, G.D.; Ren, Z.Y.; Zhang, W.; Tang, J.Q.; Zhang, L.; Si, X.L.; Zhao, Z.M. Mixed-mode I-II mesoscale fracture behavior of concrete determined by the realistic aggregate numerical model. *Constr. Build. Mater.* **2019**, *226*, 802–817. [[CrossRef](#)]
8. Loria, L.; Sebaaly, P.E.; Hajj, E.Y. Long-Term Performance of Reflective Cracking Mitigation Techniques in Nevada. *J. Transp. Res. Board.* **2008**, *2044*, 86–95. [[CrossRef](#)]
9. Morian, D.A.; Oswalt, J.; Deodhar, A. Experience with Cold In-Place Recycling as a Reflective Crack Control Technique: Twenty Years Later. *Transp. Res. Rec.* **2004**, *1869*, 47–55. [[CrossRef](#)]
10. Zhang, J.L.; Zheng, M.L.; Pei, J.Z.; Zhang, J.P.; Li, R. Research on Low Temperature Performance of Emulsified Asphalt Cold Recycled Mixture and Improvement Measures Based on Fracture Energy. *Materials* **2020**, *13*, 3176. [[CrossRef](#)]
11. Wang, D.C.; Hao, P.W.; Li, R.X.; Liu, N. Experimental study on low temperature crack resistance of emulsified asphalt cold recycled mixture. *J. Wuhan Univ. Technol. Trans. Sci. Ed.* **2020**, *44*, 64–68. [[CrossRef](#)]
12. Barghabany, P.; Cao, W.; Mohammad, L.N.; Cooper, S.B., III; Cooper, S.B., Jr. Relationships among Chemistry, Rheology, and Fracture/Fatigue Performance of Recovered Asphalt Binders and Asphalt Mixtures Containing Reclaimed Asphalt Pavement. *Transp. Res. Rec.* **2020**, *2674*, 927–938. [[CrossRef](#)]
13. Ma, Q. Study on Crack Resistance of RAP Cold Recycled Mixture. *China J. Foreign Highw.* **2016**, *36*, 284–287. [[CrossRef](#)]
14. Flores, G.; Gallego, J.; Miranda, L.; Marcobal, J.R. Cold asphalt mix with emulsion and 100% rap: Compaction energy and influence of emulsion and cement content. *Constr. Build. Mater.* **2020**, *250*, 118804. [[CrossRef](#)]
15. Zhang, R.H.; Sias, J.E.; Dave, E.V.; Rahbar-Rastegar, R. Impact of Aging on the Viscoelastic Properties and Cracking Behavior of Asphalt Mixtures. *Transport. Res. Rec.* **2019**, *2673*, 406–415. [[CrossRef](#)]
16. Feng, D.C.; Cui, S.T.; Yi, J.Y.; Chen, Z.G.; Qin, W.J. Research on low temperature performance evaluation index of asphalt mixture based on SCB test. *China J. Highw. Transp.* **2020**, *33*, 50–57. [[CrossRef](#)]
17. Chen, J.; Huang, X.M. Analysis of the influence of aggregate distribution characteristics on the fatigue performance of mixtures. *J. Build. Mater.* **2009**, *12*, 442–447. [[CrossRef](#)]
18. Li, Z.; Wang, Z.S.; Deng, Z.G.; Wu, W.L.; Sun, Y.Y. 3D simulation design and virtual shear test of asphalt mixture. *J. Tongji Univ. Nat. Sci.* **2018**, *46*, 1049–1056. [[CrossRef](#)]
19. Liu, Y.; Zhou, X.D.; You, Z.P.; Yao, S.; Gong, F.Y.; Wang, H.N. Discrete element modeling of realistic particle shapes in stone-based mixtures through MATLAB-based imaging process. *Constr. Build. Mater.* **2017**, *143*, 169–178. [[CrossRef](#)]
20. Yan, K.Z.; Ge, D.D.; You, L.Y. Microscopic analysis of uniaxial penetration shear test of asphalt mixture. *J. Hunan City Univ. Nat. Sci.* **2015**, *42*, 113–119. [[CrossRef](#)]
21. Ma, T.; Zhang, D.Y.; Zhang, Y.; Wang, S.Q.; Huang, X.M. Simulation of wheel tracking test for asphalt mixture using discrete element modelling. *Road. Mater. Pavement.* **2018**, *19*, 367–384. [[CrossRef](#)]
22. Chang, M.F.; Sheng, Y.P.; Niu, X.B.; Zhang, J.; Wang, X.R. Mesoscopic analysis of contact force chain and displacement field between asphalt mixture particles. *Mater. Rev.* **2015**, *29*, 153–156. [[CrossRef](#)]
23. Wu, W.L.; Tu, Z.X.; Li, Z. Based on the discrete element method, the influence of segregation on the structural characteristics of the mixture skeleton. *J. Guangxi Univ. Nat. Sci. Ed.* **2018**, *43*, 2303–2310. [[CrossRef](#)]
24. Liu, W.D.; Gao, Y.; Huang, X.M.; Tian, B. Analysis of meso-characteristics of in-situ compaction of asphalt pavement. *J. Harbin Inst. Technol. (Chin. Ed.)* **2019**, *51*, 99–106. [[CrossRef](#)]
25. Shi, L.W.; Wang, D.Y.; Xu, C.; Liang, H.H. Study on meso-performance of asphalt mixture skeleton based on discrete element method. *J. South China Univ. Technol. Nat. Sci.* **2015**, *43*, 50–56. [[CrossRef](#)]
26. Zhang, D.Y.; Huang, X.M.; Gao, Y. Three-dimensional discrete element virtual uniaxial creep test of asphalt mixture. *J. South China Univ. Technol. Nat. Sci.* **2012**, *40*, 15–20. [[CrossRef](#)]
27. Yu, H.N.; Shen, S.H. A micromechanical based three-dimensional DEM approach to characterize the complex modulus of asphalt mixtures. *Constr. Build. Mater.* **2013**, *38*, 1089–1096. [[CrossRef](#)]
28. Huang, K.; Xu, T.; Li, G.F.; Jiang, R.L. The feasibility of DEM to analyze the temperature field of asphalt mixture. *Constr. Build. Mater.* **2016**, *106*, 592–599. [[CrossRef](#)]
29. Buttlar, W.G.; You, Z. Discrete Element Modeling of Asphalt Concrete: Microfabric Approach. *Transp. Res. Rec.* **2001**, *1757*, 111–118. [[CrossRef](#)]
30. Barghabany, P.; Zhang, J.; Mohammad, L.N.; Cooper, S.B., III; Cooper, S.B., Jr. Novel Model to Predict Critical Strain Energy Release Rate in Semi-Circular Bend Test as Fracture Parameter for Asphalt Mixtures Using an Artificial Neural Network Approach. *Transp. Res. Rec.* **2022**, *2676*, 388–400. [[CrossRef](#)]
31. *JTG/T 5521-2019*; Technical Specification for Highway Asphalt Pavement Recycling. People’s Transportation Press: Beijing, China, 2019.
32. *JTG F40-2004*; Technical Specification for Construction of Highway Asphalt Pavements. People’s Transportation Press: Beijing, China, 2004.

33. *JTG E20-2011*; Standard Test Methods of Bitumen and Bituminous Mixtures for Highway Engineering. People's Transportation Press: Beijing, China, 2011.
34. Ding, X.H.; Ma, T.; Gao, W. Morphological characterization and mechanical analysis for coarse aggregate skeleton of asphalt mixture based on discrete-element modeling. *Constr. Build. Mater.* **2017**, *154*, 1048–1061. [[CrossRef](#)]
35. Xue, B.; Pei, J.Z.; Zhou, B.C.; Zhang, J.P.; Li, R.; Guo, F.C. Using random heterogeneous DEM model to simulate the SCB fracture behavior of asphalt concrete. *Constr. Build. Mater.* **2020**, *236*, 117580. [[CrossRef](#)]
36. Gao, L. Crack Development Behavior and Crack Resistance Mechanism of Emulsified Asphalt Cold Recycled Mixture. Ph.D. Thesis, Jiangsu Southeast University, Nanjing, China, 2016. [[CrossRef](#)]
37. Luan, Y.C.; Chen, T.; Ma, T.; Ma, Y.; Wang, N. Fracture performance analysis of cold recycled mixture based on refined DEM modeling. *China J. Highw. Transp.* **2021**, *34*, 125–134. [[CrossRef](#)]
38. Gong, F.Y.; Zhou, X.D.; You, Z.P.; Liu, Y.; Chen, S.Y. Using discrete element models to track movement of coarse aggregates during compaction of asphalt mixture. *Constr. Build. Mater.* **2018**, *189*, 338–351. [[CrossRef](#)]
39. Ma, T.; Zhang, D.Y.; Zhang, Y.; Zhao, Y.L.; Huang, X.M. Effect of air voids on the high-temperature creep behavior of asphalt mixture based on three-dimensional discrete element modeling. *Mater. Des.* **2016**, *89*, 304–313. [[CrossRef](#)]
40. Yang, Y.H.; Yue, L.; Cui, H.; Yang, Y. Simulation and evaluation of fatigue damage of cold recycled mixtures with bitumen emulsion. *Constr. Build. Mater.* **2023**, *364*, 129976. [[CrossRef](#)]
41. Zhou, X.D.; Chen, S.Y.; Ge, D.D.; Jin, D.Z.; You, Z.P. Investigation of asphalt mixture internal structure consistency in accelerated discrete element models. *Constr. Build. Mater.* **2020**, *244*, 118272. [[CrossRef](#)]
42. Qian, G.P.; Hu, K.K.; Li, J.; Bai, X.P.; Li, N.Y. Compaction process tracking for asphalt mixture using discrete element method. *Constr. Build. Mater.* **2020**, *235*, 117478. [[CrossRef](#)]
43. Wang, H.; Huang, W.L.; Cheng, J.J.; Ye, G. Mesoscopic creep mechanism of asphalt mixture based on discrete element method. *Constr. Build. Mater.* **2021**, *272*, 121932. [[CrossRef](#)]
44. Yang, Y.H.; Li, B.C.; Yang, Y.; Chen, Y.M.; Zhang, L.L. Micro-damage characteristics of cold recycled mixture under freeze–thaw cycles based on discrete-element modeling. *Constr. Build. Mater.* **2023**, *409*, 133957. [[CrossRef](#)]
45. Wang, L.; Shan, M.Y.; Li, C. The cracking characteristics of the polymer-modified asphalt mixture before and after aging based on the digital image correlation technology. *Constr. Build. Mater.* **2020**, *260*, 119802. [[CrossRef](#)]
46. Al Khateeb, L.; Anupam, K.; Erkens, S.; Scarpas, T. Micromechanical simulation of porous asphalt mixture compaction using discrete element method (DEM). *Constr. Build. Mater.* **2021**, *301*, 124305. [[CrossRef](#)]
47. Gao, L.; Zhang, Y.; Liu, Y.P.; Wang, Z.Q.; Ji, X. Study on the cracking behavior of asphalt mixture by discrete element modeling with real aggregate morphology. *Constr. Build. Mater.* **2023**, *368*, 130406. [[CrossRef](#)]
48. Zhao, X.K.; Dong, Q.; Chen, X.Q.; Ni, F.J. Meso-cracking characteristics of rubberized cement-stabilized aggregate by discrete element method. *J. Clean. Prod.* **2021**, *316*, 128374. [[CrossRef](#)]

**Disclaimer/Publisher's Note:** The statements, opinions and data contained in all publications are solely those of the individual author(s) and contributor(s) and not of MDPI and/or the editor(s). MDPI and/or the editor(s) disclaim responsibility for any injury to people or property resulting from any ideas, methods, instructions or products referred to in the content.